Soft Matter

Adhesion of flat-ended pillars with non-circular contacts

Journal:	*Soft Matter*
Manuscript ID	SM-ART-06-2020-001105.R1
Article Type:	Paper
Date Submitted by the Author:	17-Aug-2020
Complete List of Authors:	Luo, Aoyi; University of Pennsylvania Mohammadi Nasab, Amir; Yale University, Mechanical Engineering and Materials Science Tatari, Milad; University of Nevada Reno Chen, Shuai; Syracuse University Shan, Wanliang; Syracuse University Turner, Kevin; University of Pennsylvania, Mechanical Engineering and Applied Mechanics

Adhesion of flat-ended pillars with non-circular contacts†

Aoyi Luo,‡[a] Amir Mohammadi Nasab,‡[b] Milad Tatari,[b] Shuai Chen,[bc]
Wanliang Shan*[bc] and Kevin T. Turner*[a]

ABSTRACT

Fibrillar adhesives composed of fibers with non-circular cross-sections and contacts, including squares and rectangles, offer advantages that include larger real contact area when arranged in arrays and simplicity in fabrication. However, they typically have lower adhesion strength compared to circular pillars due a stress concentration at the corner of the non-circular contact. We investigate the adhesion of composite pillars with circular, square and rectangular cross-sections each consisting of a stiff pillar terminated by a thin compliant layer at the tip. Finite element mechanics modeling is used to assess differences in the stress distribution at the interface for the different geometries and the adhesion strength of different shape pillars is measured in experiments. The composite fibrillar structure results in a favorable stress distribution on the adhered interface that shifts the crack initiation site away from the edge for all of the cross-sectional contact shapes studied. The highest adhesion strength achieved among the square and rectangular composite pillars with various tip layer thicknesses is approximately 65 kPa. This is comparable to the highest strength measured for circular composite pillars and is about 6.5× higher than the adhesion strength of a homogenous square or rectangular pillar. The results suggest that a composite fibrillar adhesive structure with a local stress concentration at a corner can achieve comparable adhesion strength to a fibrillar structure without such local stress concentrations if the magnitude of the corner stress concentrations are sufficiently small such

[a] Department of Mechanical Engineering and Applied Mechanics, University of Pennsylvania, 220 South 33rd Street, Philadelphia, Pennsylvania 19104, USA. E-mail: kturner@seas.upenn.edu

[b] Mechanical Engineering Department, University of Nevada, Reno, 1664 N. Virginia Street, Reno, Nevada 89557, USA.

[c] Department of Mechanical and Aerospace Engineering, Syracuse University, Syracuse, NY 13244, USA. E-mail: washan@syr.edu.

†Electronic supplementary information (ESI) available.

‡ Authors have contributed equally.

that failure does not initiate near the corners, and the magnitude of the peak interface stress away from the edge and the tip layer thickness are comparable.

1. Introduction

Fibrillar adhesives with enhanced and repeatable adhesion via secondary bonds, including van der Waals forces, have applications ranging from robotic grasping in manufacturing[1,2] to climbing robots[3] to micro-transfer printing[4–6]. To enhance the adhesion of an individual fiber in a fibrillar adhesive, the shape and composition of the fiber can be tailored to offer a more uniform stress distribution at the adhered interface. Geckos have been the main source of inspiration from nature[7–18] to achieve enhanced dry adhesion. Mushroom-shaped fibers, which mimic the spatula-shaped structures on the Geckos' foot, redistribute stress at the adhered interfaces, resulting in high effective adhesion strength.[19] This has been demonstrated in synthetic fibers and pillar structures with dimensions on the order of micrometers[4,20] and millimeters[13].

Elastic heterogeneity has also been used to increase the dry adhesion strength of fibers to surfaces.[14,21] Composite pillars consisting of a stiff core and a soft shell were shown to result in a favorable stress distribution at the adhered interface and an increase in effective adhesion strength.[22–25] The location of the highest stress at the adhered interface depends on the thickness of the soft shell/layer of the composite pillar, t, relative to the pillar radius R, the ratio of the Young's modulus of the core and shell, and the shape of the core.[21–23] Experimental studies of various types of composite pillars have shown adhesion enhancements from 3× to 9× on millimeter and sub-millimeter pillars depending on the geometry, Young's modulus ratio, and size.[21–24] Recently, heterogeneous fibers with high adhesion strength have also been found in

nature; specifically the Setae of the ladybird beetle have a significant modulus gradient with the base being about 10^5 stiffer than the tip.[26]

While fibrillar adhesives have been extensively studied and it is widely acknowledged that the size and longitudinal shape (e.g. flat-ended pillar, mushroom, spherical tip, etc.) of the fibrillar adhesives significantly affect the adhesion strength,[17,20,27–30] little attention has been paid to the effect of the cross-sectional contact shape of the fibers on the adhesion strength. Most fibrillar adhesives in nature have axisymmetric cross-sections and contact shapes;[12] similarly most artificial fibrillar adhesives are also comprised of fibers with circular cross-sections and contact shapes.[20,31] There are only a few reports of fibers with non-circular contact areas. Kwak et al.[32] studied fiber arrays with triangular contacts to achieve directionally-dependent shear adhesion. Kim et al.[4] reported square mushroom-shaped posts and Minsky and Turner[24] reported composite pillars with square cross-sections. In both of these reports, square contacts were used to match the shape of the semiconductor chips in a microtransfer printing process. The main advantage of circular contact over others is that fibers with non-circular/elliptical contacts generally have corners at which there are stress concentrations that facilitate crack initiation at low loads. Stress concentrations are widely observed and considered in design in many structural applications. For example, a square joint is commonly observed to fail at the corner and thus it is common practice to add a fillet to the corner to reduce the stress concentration.[33,34] However, fibrillar adhesives with non-circular contacts, especially square or rectangle, have advantages. First, in many applications, arrays of fibers rather than a single fiber are needed. Square or rectangle fibers can be more closely packed and have a larger real contact area compared to fibers with circular contacts. Second, in pick-and-place applications, such as microtransfer printing of semiconductor chips, the components being manipulated are often squares or rectangles and it is desirable to match the shape of the components.[6,35] Moreover, square or rectangular fibers allow alternative fabrication methods, such as cutting along straight lines, to be used to produce fiber arrays from simple flat sheets. Thus, it is important to understand the

adhesion strength of fibers with non-circular cross sections and contact areas, and identify approaches to enhance the adhesion strength of these fibers.

In this study, composite pillars[21–25] with different cross-sectional contact shapes are investigated through finite element (FE) mechanics models and experiments. The structures studied are shown in Fig. 1 and consist of PDMS pillar (Young's modulus of 2 MPa) terminated by a thin layer of more compliant Ecoflex-50 (Young's modulus of 47 kPa) at the tip. Pillars with circular, square and rectangular cross-sections (Fig. 1(b)) are investigated. The experiments were carried out on pillars with characteristic widths of a few millimeters; these pillars are larger than typical fibers in fibrillar adhesives but were used here because they allow for detailed observation of the failure process at the interface, thus facilitating a fundamental understanding of the adhesion mechanics.

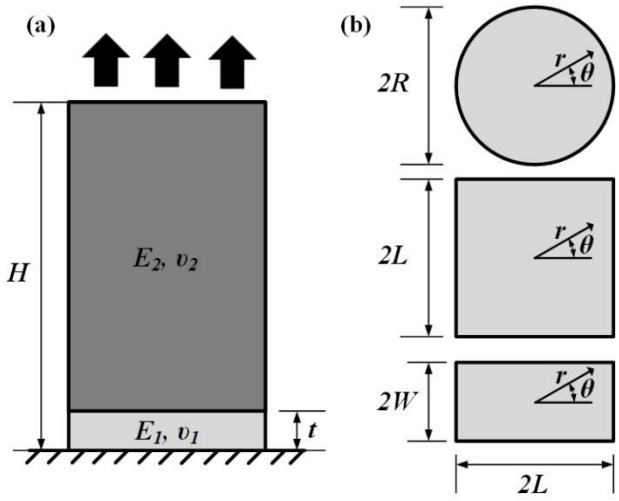

Fig. 1 Pillar geometries considered (the dark gray region is stiffer than the light gray region): (a) Side view of the pillars (b) Different cross-sectional contact shapes: circular, square and rectangular.

2. Materials and methods

2.1. Pillar fabrication

The composite pillars are made of two soft materials commonly used in soft robotics applications: Ecoflex-50 and PDMS.[36] A thin Ecoflex layer is attached to a stiffer PDMS pillar to form the composite structure. Fig. 2 shows the fabrication process for a PDMS pillar (Sylgard 184, 10:1, Dow Corning Corporation) terminated by a thin Ecoflex layer (1:1, Smooth-On, Inc.). Both uncured elastomers undergo centrifugal mixing and degassing before casting. First, a thin layer of PDMS is spin-coated on a thick aluminum wafer (chosen because of subsequent CO_2 laser patterning process) and cured at 90°C for one hour. A layer of Ecoflex-50 is then spin-coated onto the cured PDMS layer under different spinning conditions to obtain samples with a range of thicknesses (105 μm to 462 μm). The Ecoflex-50 layer is cured at 80℃ for 20 minutes and then covered with VHB adhesive tape (3M, Inc.) to protect the surface during the subsequent laser patterning step. The layer stack is patterned with a CO_2 laser (Epilog Helix 24, 75 Watts) (Figs. S1 and S2 show images of the laser cut Ecoflex-PDMS layer). Partially cured PDMS is used to bond the composite structure to a homogenous PDMS pillar that was molded separately. The structure is assembled, pressed together, and cured at room temperature for 24 hours. Finally, the VHB tape is removed. Pillars with circular (R=3.5 mm), square (L=3.5 mm) and rectangular (W=1.75 mm and L=4.2 mm) cross-sections and overall height H=12 mm were fabricated. Fig. 2(c) shows an image of a typical fabricated structure with rectangular cross-section.

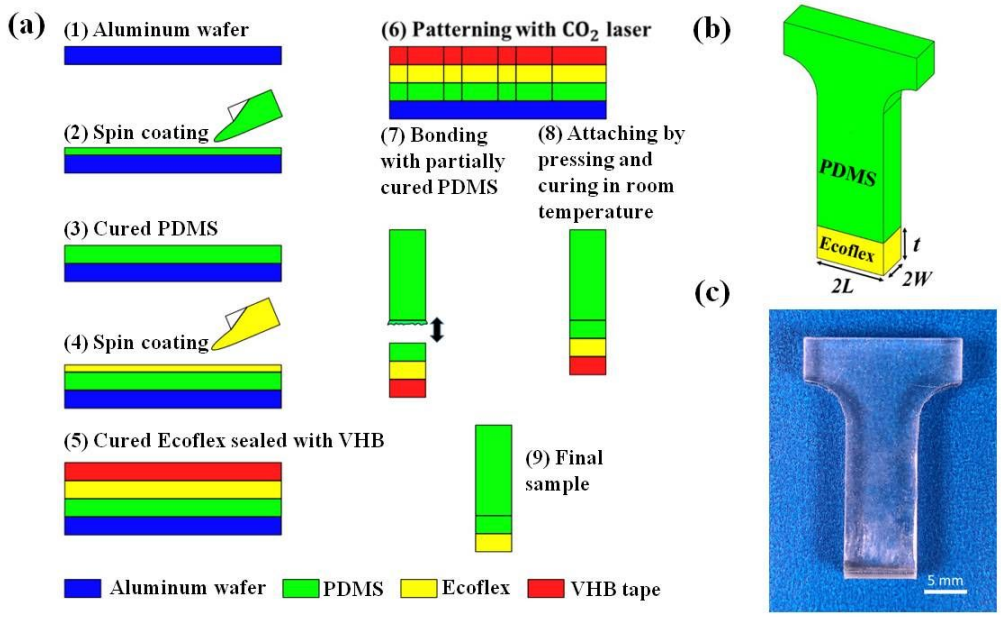

Fig. 2 (a) Composite pillar fabrication process. (b) Schematic of a rectangular composite pillar. (c) Picture of a rectangular composite pillar.

2.2. Adhesion tests

The maximum adhesion force (i.e. pull-off force) between each composite pillar and a standard glass microscope slide were measured using an Instron 5969 test system with a 50 N load cell. The composite pillar was mounted using a 3D-printed fixture and displaced normal to the glass substrate in displacement control. In all tests, the pillar was brought into contact at a rate of 2 μm/s, held at a compressive preload of 60 kPa for 2 minutes, and then retracted at 20 μm/s. The pull-off force was defined as the peak force measured during retraction. The crack initiation and propagation during pillar detachment from the glass substrate were imaged using a digital camera. The camera was placed below the glass such that the pillar-glass interface could be imaged.

Throughout this paper, the "adhesion strength" of pillars is calculated as $\sigma_{adh} = F_P/A$, where F_P is the measured pull-off force and A is the nominal contact area of the pillar. This adhesion strength represents the average stress on the interface at pull off and is not an intrinsic property of the interface as the stress distribution at the interface is non-uniform; regardless it provides a useful measure of the load capacity of the pillar per area which is of primary interest in applications of dry adhesives. Many previous reports on the adhesion of pillar and fiber contacts also describe performance in terms of adhesion strength as is done here.[21–25]

2.3. Finite element modeling

FE modeling was performed using Abaqus Standard (Abaqus 2016, Providence, RI) to investigate the stress distribution at the adhered interface for pillars with different cross-section geometries. Composite pillars shown in Fig. 1 with overall height H=12 mm and compliant tip layers with thickness, t, varying from 70 μm to 6.65 mm, were investigated. Simulations were also run for homogenous pillars (since the interfacial stress distribution is independent of the Young's modulus, the stress distributions are the same for homogenous compliant (H=t=12 mm) and homogenous stiff pillars (H=12 mm, t=0 mm)). Pillars with circle (R=3.5 mm), square (L=3.5 mm) and rectangle (W=1.75 mm and L=4.2 mm) cross sections were considered. A 2D

axisymmetric model was used for the circular pillars and 3D models were used for the square and rectangular pillars. Materials are modeled as linear elastic: the Young's modulus and Poisson ratio of compliant tip layer is E_1=72 kPa, v_1=0.499 (Ecoflex-50) and the Young's modulus and Poisson ratio of stiff portion of the pillar is E_2=2 MPa, v_2=0.499 (PDMS)[22,24]. Note, Ecoflex is a hyperelastic material and, thus the behavior may deviate from a linear elastic model at high strains. A comparison between a hyperelastic and linear elastic model for circular pillars is shown in Fig. S3. The results in Fig. S3 show that the trend in stress distribution as a function of t/R is not significantly different for the two constitutive models, thus the discussion in the manuscript is limited to linear elastic results. The bottom interface of the pillar is fixed in all directions to model adhesion to a rigid flat substrate. The top interface of the pillar was displaced equally in the z-direction with no other displacement allowed which simulates the condition of the pillar being attached to a rigid support plate. Axisymmetric quadrilateral elements (CAX4H) were used to mesh the axisymmetric models for the circular pillars and 3D hexahedral elements (C3D8H) were used to mesh the 3D models for the square and rectangular pillars. For all models, the mesh near the contact interface and the free edge was refined, and mesh convergence was performed with further refinement resulting in less than 0.3% difference in the average normal stress. Approximately 1.3×10^5 to 4.3×10^5 elements were used over the range of layer thickness studied here for the 2D axisymmetric model and approximately 3.2×10^5 to 6.3×10^5 elements were used for the 3D models.

Generally, for an adhered pillar structure, a high stress is generated at the edge of the interface in the form of stress with a singularity described as $\sigma_{zz}=Kd^n$, where K is the magnitude of singularity, d is the distance from the edge and n is a negative exponent ranging from -0.5 to 0.[37] Failure is often observed to initiate from this singularity dominated region and the magnitude of the singularity, K, is widely used as a failure criterion to predict edge-initiated failure.[25,37–43]

3. Results and discussion

3.1. Circular pillars

The results for pillars with circular contacts, as they are the most extensively studied fibrillar geometry in the literature, are presented first. Fig. 3(a) shows the experimentally measured

adhesion strength and experimentally observed location of crack initiation as a function of t/R for pillars with circular contacts. As t/R decreases from 3.4 (which corresponds to a homogenous Ecoflex pillar) to 0.034, the measured adhesion strength first increases then decreases; the maximum adhesion strength of 65 kPa is achieved at t/R=0.06 which is 5.7× higher than that of a homogenous Ecoflex circular pillar. Moreover, in the experiments, the location of crack initiation is observed to shift from the edge to the center and finally to a location between the center and edge as t/R is decreased. It has been observed that the thickness of a confined soft layer can change the interfacial failure mode and that failure can occur from an edge crack, an internal crack, cavitation, or fingering.[44] Such a change in failure mechanism was reported in past studies for composite pillars. Fischer et al.[23] and Balijepalli et al.[25] observed a drop in adhesion strength when the failure mode changed from an edge crack to fingering as the tip layer thickness was reduced. A change of the failure mechanism from an edge crack to an internal crack has also been previously observed with decreasing tip layer thickness, resulting in an increase in adhesion strength.[22,23,25] Here, we also observe a change in failure mechanism from an edge crack to an internal crack, but we observe a non-monotonic trend in adhesion strength with tip layer thickness in the regime where failure occurs via an internal crack.

As the normal stress distribution at the interface is critical for determining adhesion strength,[17,22,27,28,45] we show FE-calculated normal stress distributions at the interface for various t/R in Fig. 3(b) to understand the behavior observed in experiments. The stress distribution near edge of the pillar contact is replotted in Fig. 3(c) on a logarithmic scale to highlight the details of the stress singularity near the edge. The linear region in this logarithmic plot indicates the edge singularity dominated region, and the slope and intercept of this line on this logarithmic scale are n and log$K$ in the aforementioned equation: $\sigma_{zz}=Kd^n$.[25,37]

When t/R is reduced from 3.43 to ~0.15, the normal stress is reduced near the contact edge and is increased in the center of the contact (Fig. 3(b) and 3(c)). The experimentally observed increase in adhesion strength and shift in crack initiation site from edge to center as t/R decreases to ~0.15 is due to this redistribution of the stress as noted in past studies.[22,25] For t/R less than ~0.15, the normal stress near the edge is relatively insensitive to t/R (Fig. 3(c)), but the stress at the center of the pillar decreases with decreasing t/R (Fig. 3(b)). When $t/R \leq$~0.06, a local maximum in the stress is observed at a site between the edge and the center. With decreasing t/R

below 0.06, the magnitude of the stress at the local maximum increases and the location of the local maximum moves towards the edge. As discussed in supporting information (eqs. S1 to S5), the adhesion strength can be increased by having the crack initiate at an internal site away from the edge, minimizing the magnitude of the peak stress away from the edge, and reducing the thickness of the soft layer. For the circular composite pillar with the highest adhesion strength, t/R=0.06, the stress near the edge is sufficiently low for the crack to initiate away from the edge, as observed in the experiments. Moreover, the t/R=0.06 pillar also has the lowest internal peak stress among all the t/R investigated (see Fig. 3(b)). Decreasing t/R below 0.06 results in a thinner tip layer but the peak stress away from the edge increases and the position of the local maximum moves closer to the edge (Fig. 3(b)). This leads to a reduction of the adhesion strength, as observed in experiments at t/R<0.06. Additional FE simulations show that the trend of the stress distribution as a function of t/R is similar for composite pillars with different elastic modulus ratios, but the value of t/R to reach a specific stress distribution decreases as the elastic modulus mismatch of the materials increases (Fig. S4). From both experiment and FE results, it is evident that the adhesion strength of composite circular pillars does not change monotonically with t/R and that there is an optimal t/R ratio. As eq. S1 suggests, the crack initiation position and the exact t/R ratios that divide the three crack initiation regimes (i.e., edge, center, between edge and center) are determined by both the stress distribution and the initial defect distribution at the interfaces which depend on various factors including material properties, fabrication precision and substrate roughness.[22,24]

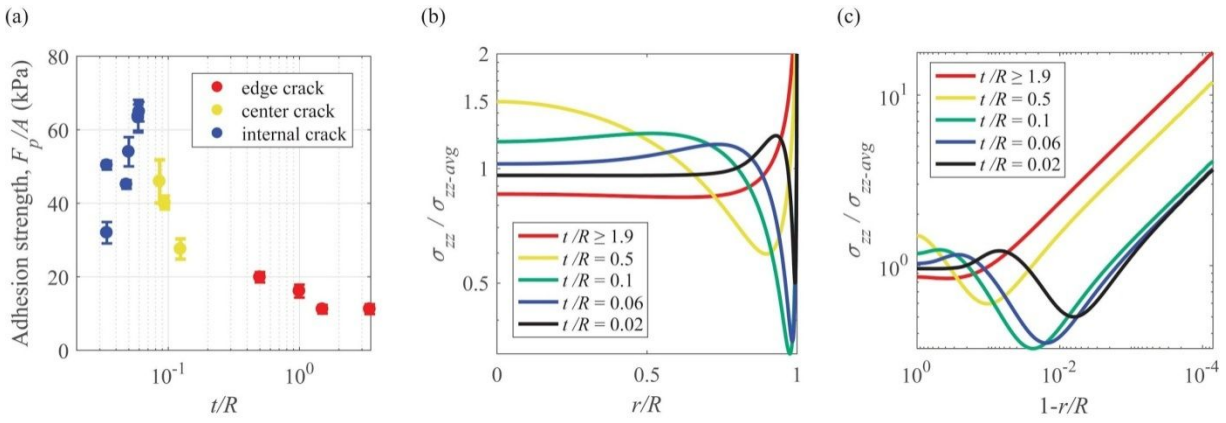

Fig. 3. Experimental and FE results for pillars with circular contacts with different t/R ratios: (a) Experimentally measured adhesion strength, which is calculated as the pull-force divided by the nominal contact area (Experimentally observed location of crack initiation is denoted by

different colors as marked in the legend). (b) Normal stress distribution at the adhered interface. (c) Normal stress distribution at the adhered interface near the edge.

3.2. Square and rectangular pillars

The FE-calculated normal stress distributions at the adhered interface for composite square and rectangular pillars with various *t/L* ratios are shown in Fig. 4. Due to the symmetry of the square and rectangular pillars, only a quarter of the pillar was simulated and is shown. The normal stress distributions in Fig. 4 demonstrate that the value of the *t*/*L* modifies the overall stress distribution at the adhered interface for a pillar with non-circular contact and the trend is similar to that of a circular pillar (Fig. 3). The stress at the center increases as *t*/*L* is reduced and further reduction beyond a critical *t*/*L* then leads to a higher peak stress at a location between the center and the edge. Since the main difference between a circular pillar and a square pillar is the presence of the sharp corner, the normal stress distributions along a diagonal line (θ=45°) from the center of the square pillars is shown in Fig. 5 to give insight into the stress near the corner. The normal stress distributions along the axis of the symmetry passing through the mid-edge points (i.e. a line from the center at θ=0°) of the square are also shown in Fig. 5. Notably, the stress distributions along the center line of the square (θ=0°) (Fig. 5) are nearly the same as those for a circular pillar (Fig. 3) for *t*/*R*=*t*/*L*. The changes to the stress distributions with varying *t*/*L* along the diagonal line (Fig. 5(a) and (b)) are similar to changes in the stress distribution along the center line (Fig. 5(c) and (d)) of square pillars and circular pillars with varying *t*/*R* (Fig. 3), and the stress near corner is reduced by reducing *t*/*L*. This indicates that a square or rectangular composite pillar with a sufficiently small *t/L* can have enhanced adhesion compared to a homogenous pillar with same cross-section geometry.

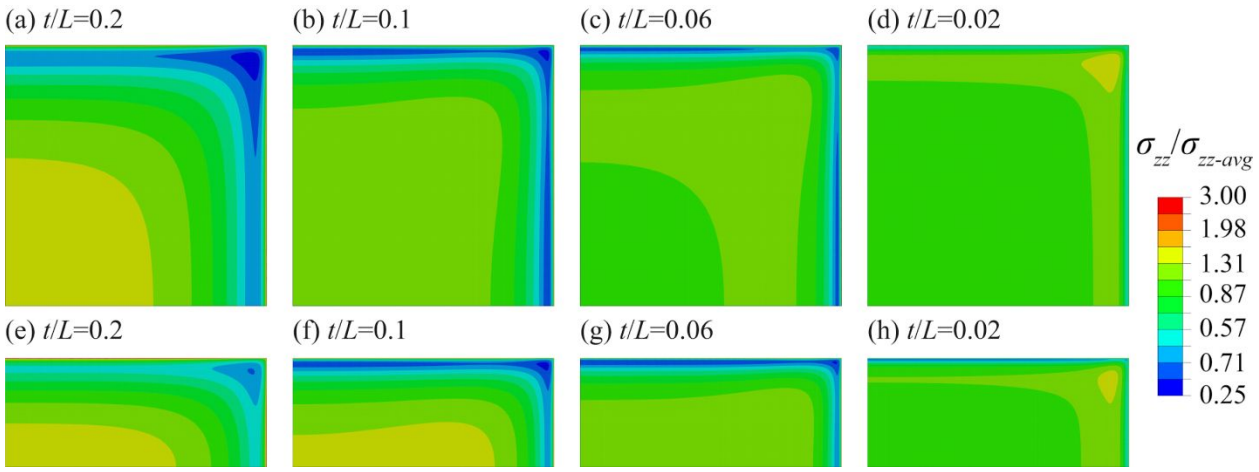

Fig. 4 Normal stress distribution at the adhered interface of pillars with (a)-(d) square and (e)-(h) rectangular contacts (W=0.42L). One quarter of the pillar is shown. Results for different t/L ratios (left and bottom boundaries represent symmetry): (a) and (e) t/L= 0.2. (b) and (f) t/L= 0.1. (c) and (g) t/L= 0.06. (d) and (h) t/L= 0.02. Note: Color scale is logarithmic.

While the above suggests a square or rectangular composite pillar can achieve enhanced adhesion relative to a homogenous pillar with the same cross-section, the square or rectangular composite pillars may still fail from the corner and have lower adhesion strength compared to a circular composite pillar. Due to presence of the sharp corner, the negative exponent n of the stress singularity in equation $\sigma_{zz}=Kd^n$ along the diagonal line is smaller than the corresponding exponent along the center line (i.e. the slope of the linear regions in Fig. 5(b) is more steep than the slope of the linear regions in Fig. 5(d)). As a result, the corner is still the highest stress concentration site on the contact perimeter of a square or rectangular composite pillar and the stress (Fig. 5(d)) is higher than the stress near edge of a circular pillar (Fig. 3(c)) for a given $t/L=t/R$. If the crack initiates at the corner, then the adhesion strength of a square or rectangular pillar is always expected to be lower than that of the corresponding composite circular pillar with $t/L=t/R$. For square or rectangular composite pillars to achieve adhesion strength comparable to the circular pillars, it is thus essential to ensure that the stress at the corner is low enough for the crack initiation site to be at a location away from the corner, and the magnitude of the peak interface stress away from the edge and the tip layer thickness are comparable. Since the above discussion is based on the effect of the interface stress distribution on adhesion strength, it provides general guidance to avoid a reduction in adhesion strength in fibrillar adhesives with local stress concentrations (e.g. non-circular contacts, local defects).

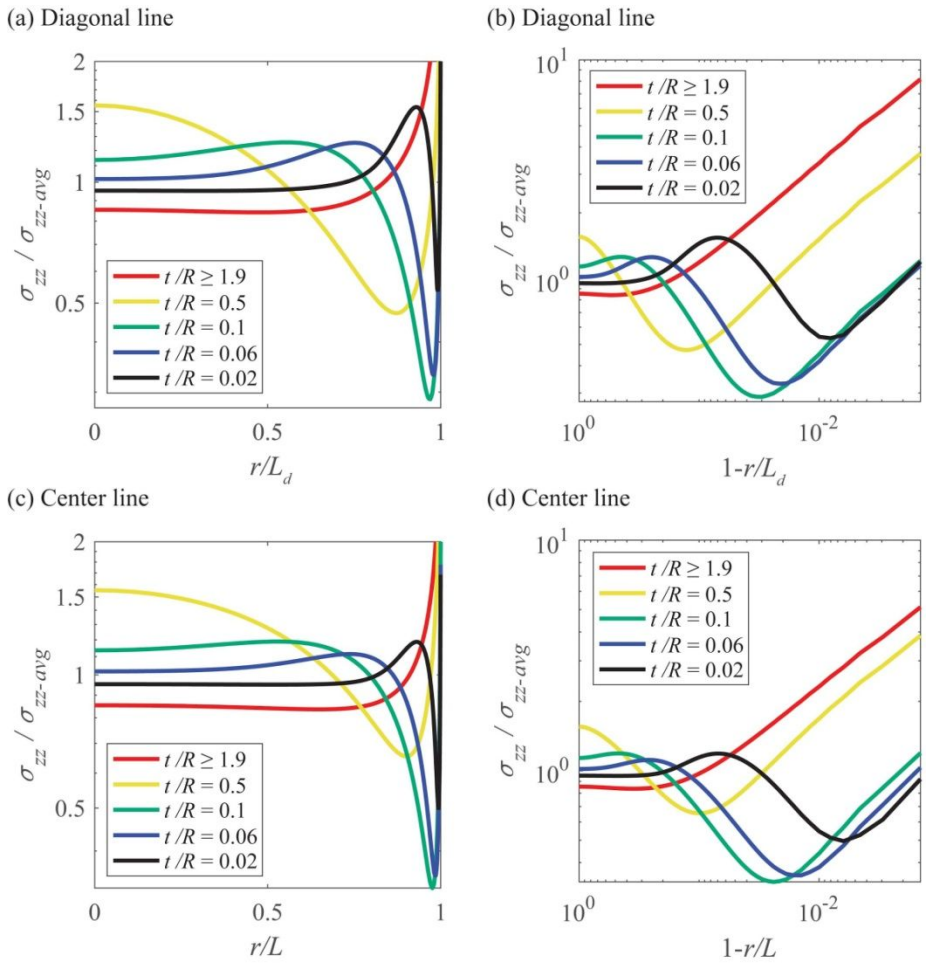

Fig. 5 Normal stress distribution at adhered interface for pillars with square contacts and various t/L: (a) Normal stress distribution along the diagonal line (θ=45°). (b) Normal stress distribution near the edge along the diagonal line (θ=45°). (c) Normal stress distribution along the center line (θ=0°). (b) Normal stress distribution near the edge along the center line (θ=0°).

Adhesion measurements were performed on square and rectangular composite pillars; results are shown in Fig. 6. Due to the similarity in the stress distribution between square or rectangular and circular pillars as discussed above, the trend in adhesion strength as a function of t/L is similar to that of circular pillars: as t/L decreases, the adhesion strength first increases then decreases and the crack initiation site shifts from edge to the center and then to a site between the center and the edge. The highest adhesion strength of 65 kPa is reached at t/L=~0.06 for both square and rectangular pillars. At this max adhesion strength, Fig. 7 shows that delamination initiates from internal points on the interface and propagates across the interface for the rectangular pillar geometry (t/L=0.06). A video of the crack initiation and propagation is included as Video S1 and it is clear that the cracks initiate at the high stress region identified in

the FE simulations (Fig. 4). The number of initial voids is higher on the left side of the images but voids also develop on the right side of the images suggesting there is a slight but not significant misalignment during testing. The highest adhesion strength of the composite square and rectangular pillars is comparable to the highest adhesion strength measured on composite circular pillars. This shows that comparable adhesion strength can be achieved as long as the crack initiation site is away from the stress concentration at the corner, and the internal peak stress and the tip layer thickness are comparable to circular composite pillars.

A square pillar provides larger contact area compared to a circular pillar for $L=R$, thus given the same adhesion strength and $L=R$, the force capacity for a square pillar is 27% higher than that of a circular pillar. Note that when the pillars are arranged in an array, the real contact area of the entire array is also affected by the spacing between pillars. As shown in Fig. S6, the ratio of the minimum spacing required for square pillars to prevent lateral sticking to the minimum spacing of circular pillars decreases as the pillar size decreases, and the minimum spacing required for square pillars becomes smaller than that of circular pillars when $L=R<1$ μm. The result suggests that a square pillar array becomes more favorable compared to a circular pillar array when the size of each individual pillar becomes smaller. Smaller pillars generally have higher adhesion strengths (the adhesion strength of the composite pillar scales with $\sqrt{G_c E/R}$ [24]) and better resistance to contamination.[46] Besides the size of the pillar, the aspect ratio of the pillar also affects the minimum spacing and thus the real contact area (Fig. S7). For short pillars (e.g. $h/R=2$), a square pillar array can always achieve higher real contact area compared to a circular pillar array regardless of the pillar size. The square and rectangular composite pillars have 6.5× adhesion enhancement relative to a homogenous ($t/R>1.9$) Ecoflex pillars with the same geometry. The homogenous ($t/L=3.4$) square and rectangular pillars that fails from the corner have an experimentally measured adhesion strength that is ~18% lower than that of a homogenous circular pillar. Thus, the enhancement ratio for square and rectangular pillars is higher than that of circular pillars. Notably, the higher change in adhesion strength indicates that square or rectangular pillars are a better geometry than circular pillars for active adhesion tuning if the stiffness of the stiff base of the pillar is actively tuned as described in our previous work.[21]

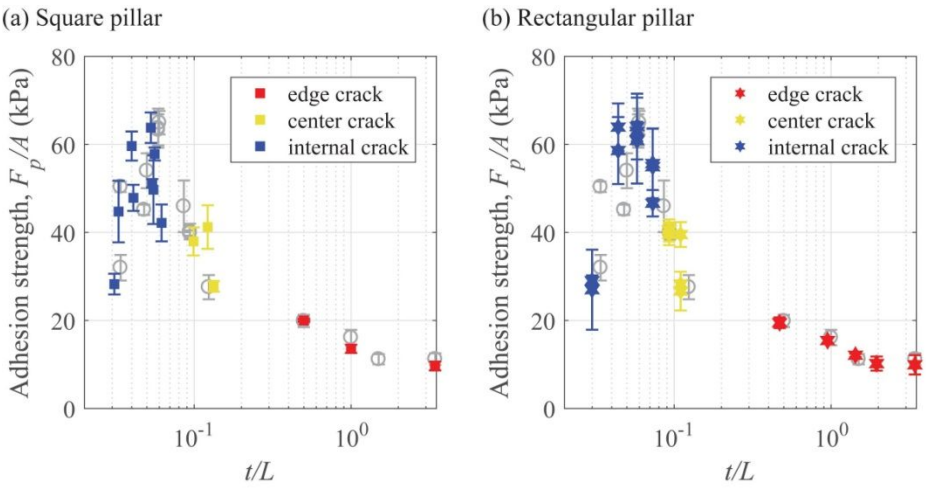

Fig. 6 Experimentally measured adhesion strength as a function of t/L: (a) square pillars. (b) rectangular pillars (W=0.42L). Circular pillar data from Fig. 3(a) with $t/R = t/L$ is shown as the gray circles for comparison. Experimentally observed location of crack initiation is denoted by different colors.

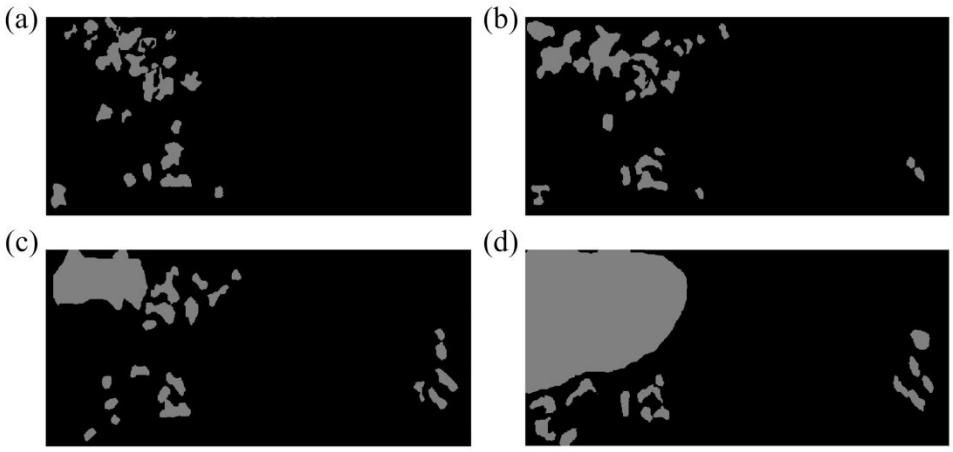

Fig. 7 A sequence of images presented as a binary black-gray image showing how failure progresses at the adhered interface for rectangular pillars with t/L=0.06. The gray regions are the regions on the interface that have delaminated, and the black regions are the regions on the interface that are in contact. The sequence of images shows different time points in the test and were chosen to show (a) nucleation, (b) growth and (c) merging of voids, ultimately resulting in (d) partial detachment and eventual interface failure. The dimensions of the adhered interface shown in each of these images is 8.4×3.5 mm. (Original images of the interface are shown in Fig. S5)

In the experiments and all other real scenarios, the corner will have a finite curvature and this may result in a lower stress near the corner compared to earlier the simulations in which a perfectly sharp corner was assumed. Moreover, in engineering applications, non-circular pillars with fillets at the corner could be intentionally designed to preserve the benefits of the non-circular pillar while avoiding the potential disadvantages of the sharp corner. It is thus important to understand the effect of corner curvature on the local stress concentration near corner and the stress distribution of square pillars with rounded corners were calculated using FE. Since the geometry is only changed near the corner, it is expected that the change in stress distribution is also limited to this region. To examine the stress distribution near the corner, the normal stress along a diagonal line (θ=45°) of square pillars with various fillet radii, R_f, are shown in Fig. 7 (the full normal stress distribution at the adhered interface is shown in Figs. S8 to S11). A circular pillar is equivalent to a square pillar with R_f/L= 1.

A smaller radius, R_f, not only indicates a sharper corner but also results in a larger diagonal length, R_d, which leads to a smaller t/R_d for a given t. Moreover, larger R_d itself results in a higher magnitude of the singularity, K, at the corner even with same normalized stress distribution ($\sigma_{zz}/\sigma_{zz\text{-}avg}$ vs. r/R_d) based on dimensional analysis in Supporting Information (eqs. S12to S15), and this means the absolute stress near the corner is higher for smaller R_f. As a result, the overall stress distribution near the corner is determined by those competing mechanisms. For a homogenous square pillar (or $t/R \geq 1.9$), a higher stress near corner is observed for square pillars with sharper corner (smaller R_f/L) as expected (Fig. 8(a)). Since a homogenous pillar fails at the corner, magnitude of singularity at corner, K, can be used to predict the adhesion strength.[25,37] The magnitude of singularity obtained from FE simulation for a homogenous circular pillar (equivalent to a homogenous square pillar with R_f/L=1) is 35% lower than that of a square pillar with R_f/L=1/16, so the adhesion of homogenous circular pillar is expected to be 35% higher than that of a square pillar with R_f/L=1/16. For small t/L (t/L=0.02 here), higher stress along diagonal line with smaller fillet radii is also observed (Fig. 8(d)). However, for intermediate t/L (t/L=0.1 and 0.06), the stress distribution along diagonal line is insensitive to the corner radii due to the combined effect of changing t/R_d in this range. From these results, it is clear that fillet radii at corners can help to reduce stress near corner, but this effect is diminished for intermediate t/L by the composite effect of smaller t/R_d.

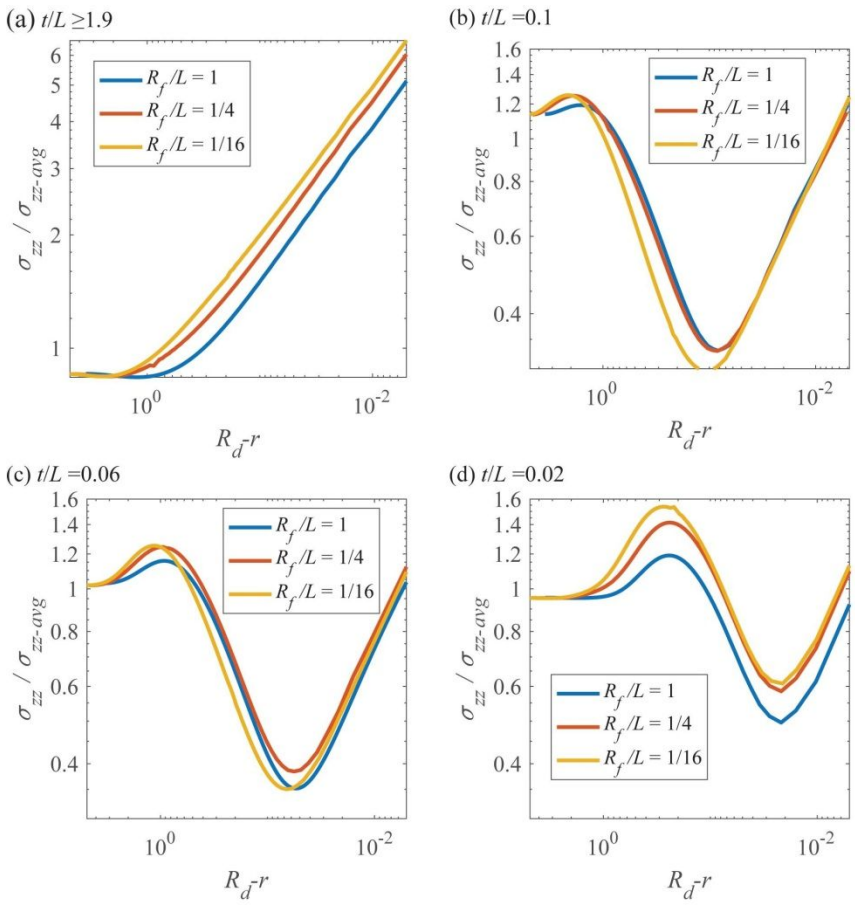

Fig. 8 Normal stress distribution of a square pillar with various fillet radii R_f/L near the edge along the diagonal line: (a) $t/L \geq 1.9$ t/L=0.1 (c) t/L=0.06 (d) t/L=0.02.

4. Conclusions

The adhesion of composite pillars with different cross-sectional contact shapes was investigated. Pillars with circular, square and rectangular cross-sections were examined through experiments and FE-based mechanics modeling. The mechanics of all three cross-section geometries show a similar dependence on the thickness of the terminating layer: as t/R (or t/L) ratio is reduced, the adhesion strength first increases and then decrease and the crack initiation site shifts from corner (or edge for circular pillars) to the center and finally to a location between the perimeter and the center. By generating a favorable stress distribution on adhered interface and shifting the crack initiation site away from the corner, square and rectangular pillars achieve the highest adhesion strength of 65kPa at t/L=~0.06, which is comparable to the highest adhesion strength achieved by composite circular pillars at t/R=0.06. This value is ~5.7· that of the

strength of a homogenous circular Ecoflex pillar and ~6.5· that of the strength of a homogenous square or rectangular Ecoflex pillar. This work provides a route to avoid a reduction of adhesion strength of fibrillar adhesives comprised of fibers with non-circular cross-sectional contact shapes.

Conflicts of interest

There are no conflicts to declare.

Acknowledgements

This work was supported by the National Science Foundation (NSF) under awards CMMI 1663037, 1830475, and 1663658.

References

1 M. Zhou, Y. Tian, D. Sameoto, X. Zhang, Y. Meng and S. Wen, *ACS Appl. Mater. Interfaces*, 2013, **5**, 10137–10144.

2 J. Purtov, M. Frensemeier and E. Kroner, *ACS Appl. Mater. Interfaces*, 2015, **7**, 24127–24135.

3 C. Menon, M. Murphy and M. Sitti, in *2004 IEEE International Conference on Robotics and Biomimetics*, IEEE, 2004, pp. 431–436.

4 S. Kim, A. Carlson, H. Cheng, S. Lee, J. K. Park, Y. Huang and J. A. Rogers, *Appl. Phys. Lett.*, 2012, **100**, 171909.

5 M. M. A. Feng X Bowen AM, Huang Y, Nuzzo RG, Rogers JA, X. Feng, M. A. Meitl, A. M. Bowen, Y. Huang, R. G. Nuzzo and J. A. Rogers, *Langmuir*, 2007, **21**, 12555–12560.

6 M. A. Meitl, Z. T. Zhu, V. Kumar, K. J. Lee, X. Feng, Y. Y. Huang, I. Adesida, R. G. Nuzzo and J. A. Rogers, *Nat. Mater.*, 2006, **5**, 33–38.

7 S. Reddy, E. Arzt and A. Del Campo, *Adv. Mater.*, 2007, **19**, 3833–3837.

8 S. Kim, M. Spenko, S. Trujillo, B. Heyneman, D. Santos and M. R. Cutkoskly, *IEEE Trans. Robot.*, 2008, **24**, 65–74.

9 C. A. Gilman, M. J. Imburgia, M. D. Bartlett, D. R. King, A. J. Crosby and D. J. Irschick, *PLoS One*, 2015, **10**, e0134604.

10 M. J. Imburgia, C. Y. Kuo, D. R. Briggs, D. J. Irschick and A. J. Crosby, *Integr. Comp. Biol.*, 2019, **59**, 182–192.

11 S. Gorb, *Attachment Devices of Insect Cuticle*, Kluwer Academic Publishers, Dordrecht, 2002.

12 S. Gorb and R. Beutel, *Naturwissenschaften*, 2001, **88**, 530–534.

13 S. N. Gorb and M. Varenberg, *J. Adhes. Sci. Technol.*, 2007, **21**, 1175–1183.

14 L. F. Boesel, C. Cremer, E. Arzt and A. Del Campo, *Adv. Mater.*, 2010, **22**, 2125–2137.

15 S. Gorb, M. Varenberg, A. Peressadko and J. Tuma, *J. R. Soc. Interface*, 2007, **4**, 271–275.

16 M. Kamperman, E. Kroner, A. Del Campo, R. M. McMeeking and E. Arzt, *Adv. Eng. Mater.*, 2010, **12**, 335–348.

17 A. V. Spuskanyuk, R. M. McMeeking, V. S. Deshpande and E. Arzt, *Acta Biomater.*, 2008, **4**, 1669–1676.

18 V. Alizadehyazdi, M. Modabberifar, S. M. Javid Mahmoudzadeh Akherat and M. Spenko, *J. R. Soc. Interface*, 2018, **15**, 20170714.

19 G. Carbone, E. Pierro and S. N. Gorb, *Soft Matter*, 2011, **7**, 5545–5552.

20 R. Hensel, K. Moh and E. Arzt, *Adv. Funct. Mater.*, 2018, **28**, 1800865.

21 M. Tatari, A. Mohammadi Nasab, K. T. Turner and W. Shan, *Adv. Mater. Interfaces*, 2018, **5**, 1800321.

22 H. K. Minsky and K. T. Turner, *Appl. Phys. Lett.*, 2015, **106**, 201604.

23 S. C. L. Fischer, E. Arzt and R. Hensel, *ACS Appl. Mater. Interfaces*, 2017, **9**, 1036–1044.

24 H. K. Minsky and K. T. Turner, *ACS Appl. Mater. Interfaces*, 2017, **9**, 18322–18327.

25 R. G. Balijepalli, S. C. L. Fischer, R. Hensel, R. M. McMeeking and E. Arzt, *J. Mech. Phys. Solids*, 2017, **99**, 357–378.

26 H. Peisker, J. Michels and S. N. Gorb, *Nat. Commun.*, 2013, **4**, 1661.

27 H. Gao and H. Yao, *Proc. Natl. Acad. Sci.*, 2004, **101**, 7851–7856.

28 T. Tang, C. Y. Hui and N. J. Glassmaker, *J. R. Soc. Interface*, 2005, **2**, 505–516.

29 G. Carbone and E. Pierro, *Small*, 2012, **8**, 1449–1454.

30 B. Aksak, K. Sahin and M. Sitti, *Beilstein J. Nanotechnol.*, 2014, **5**, 630–638.

31 M. P. Murphy, S. Kim and M. Sitti, *ACS Appl. Mater. Interfaces*, 2009, **1**, 849–855.

32 M. K. Kwak, H. E. Jeong, W. G. Bae, H. S. Jung and K. Y. Suh, *Small*, 2011, **7**, 2296–2300.

33 A. D. Christitsas, D. T. Pachoumis, C. N. Kalfas and E. G. Galoussis, *J. Constr. Steel Res.*, 2007, **63**, 1361–1372.

34 Y. Chen, R. Feng and J. Wang, *J. Constr. Steel Res.*, 2015, **106**, 234–245.

35 A. Carlson, S. Wang, P. Elvikis, P. M. Ferreira, Y. Huang and J. A. Rogers, *Adv. Funct. Mater.*, 2012, **22**, 4476–4484.

36 A. M. Nasab, A. Sabzehzar, M. Tatari, C. Majidi and W. Shan, *Soft Robot.*, 2017, **4**, 411–420.

37 S. N. Khaderi, N. A. Fleck, E. Arzt and R. M. McMeeking, *J. Mech. Phys. Solids*, 2015, **75**, 159–183.

38 A. R. Akisanya and N. A. Fleck, *Int. J. Solids Struct.*, 1997, **34**, 1645–1665.

39 R. G. Balijepalli, M. R. Begley, N. A. Fleck, R. M. McMeeking and E. Arzt, *Int. J. Solids Struct.*, 2016, **85**–**86**, 160–171.

40 A. Gradin, *J. Compos. Mater.*, 1982, **16**, 448–456.

41 H. L. Groth, *Int. J. Adhes. Adhes.*, 1988, **8**, 107–113.

42 E. D. Reedy, *Eng. Fract. Mech.*, 1990, **36**, 575–583.

43 E. D. Reedy, *Int. J. Solids Struct.*, 1993, **30**, 767–777.

44 A. J. Crosby, K. R. Shull, H. Lakrout and C. Creton, *J. Appl. Phys.*, 2000, **88**, 2956–2966.

45 A. Mohammadi Nasab, A. Luo, S. Sharifi, S. Sharifi, K. T. Turner, W. Shan and W. Shan, *ACS Appl. Mater. Interfaces*, 2020, **12**, 27717–27725.

46 W. R. Hansen and K. Autumn, *Proc. Natl. Acad. Sci.*, 2005, **102**, 385–389.

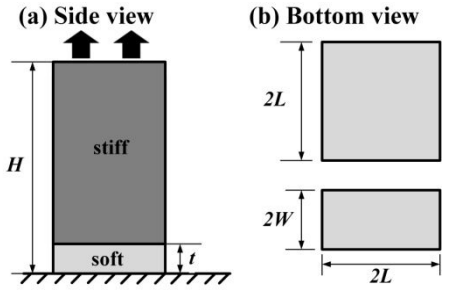

Adhesion of composite square and rectangular pillars are studied, and the highest adhesion is comparable to that of circular pillars.